MECSOL 2019 - Proceedings of the 7th International Symposium on Solid Mechanics,
V. Tita, A. Ferreira, M.L. Ribeiro, A. Vieira and A.T. Beck (Editors), ABCM, Sao Carlos, SP, Brazil, April 15th to 17th, 2019

# Free-checkerboard topology optimization using the generalized finite-volume theory

**Marcelo Vitor Oliveira Araujo [1], Eduardo Nobre Lages [1], and Márcio André Araújo Cavalcante [1]**

[1] Federal University of Alagoas, Av. Lourival Melo Mota, Tabuleiro do Martins, CEP: 57072-900, Maceió, Alagoas, Brazil

*Abstract: In the gradient-based topology optimization algorithms based on the finite-element method is very common to observe some problems related to numerical instabilities, such as checkerboard pattern, local minima and mesh dependence. Possible solutions for the checkerboard pattern and mesh dependence issues are the adoption of higher order finite elements or filtering techniques. Basically, the checkerboard pattern is directly associated with the solution assumptions of the finite-element method, as the satisfaction of equilibrium equations and the compatibility conditions among elements established through the nodes, resulting in checkerboard optimized topologies. On the other hand, the finite-volume theory satisfies the equilibrium equations in the subvolume level, and the kinematic and static compatibilities are established through the subvolume adjacent interfaces, as expected from the Continuum Mechanics point of view. In this context, different approaches of topology optimization for compliance minimization based on the generalized finite-volume theory are proposed for continuum elastic structures, resulting in computational efficient tools and leading to checkerboard-free topologies.*

***Keywords: finite-volume theory, topology optimization, checkerboard-free topologies, compliance minimization, continuum elastic structures.***

## INTRODUCTION

Topology optimization algorithms seek to establish the best material distribution in an analysis domain under an objective function and restrictions to the problem. This approach was first employed by Bendsøe and Kikuchi (1988), and, currently, it is a method that can be recognized as well-established for mechanical design of structures. This method was developed to work efficiently with strain energy, compliance minimization, or stiffness maximization. In the definition of an optimum topology, the interest is in the determination of the best solid isotropic material distribution in a given domain (Bendsøe and Sigmund, 2003). In other words, we want to define which points of the domain must be void or material, generating the so-called black-white design, usually designated by the binary 0-1, which leads to integer programming problems.

With the purpose to avoid problems of discrete optimization, the material distribution in the analysis domain can be described as a continuum function, which defines a material relative density and assumes an admissible set of values between the discrete limits: approximately 0, for void, and 1, for solid. An alternative approach, based on this assumption, is the Solid Isotropic Material with Penalization (SIMP) method. In this method, the material properties are assumed to be constant inside each element of the discretized domain, and the design variables are the element relative density. As a result, the material properties are modeled by the relative material density raised to a given power with the intention to penalize possible intermediate values of relative densities.

Topology optimization has raised as a powerful method for the design of structures, however, there still some difficulties related to numerical instabilities. According to Sigmund and Petersson (1998), the most common numerical problems can be divided in three categories: checkerboard pattern effect, which refers to the formation of regions alternating solid and void elements in a checkerboard shape; mesh dependence, which refers to the problem of not having qualitatively the same solution for different discretizations; and local minima, which refers to the problem of having different solutions for the same discretization when different input parameters are employed. Therefore, it is undesirable to have any of these instabilities in the optimal solution, especially the one related to the checkerboard pattern.

For the solution of structural problems based on the elasticity theory, it can be used some structural analysis techniques, such as finite-element method (FEM), finite difference method, contour element method, finite volume method, minimum quadratic method, and, recently, the finite-volume theory (FVT). Certainly, FEM is the most common, employed in several consolidate software packages with this purpose. As a result, its advantages and disadvantages are well-known, particularly in topology optimization.

An alternative technique to FEM is the FVT, proposed initially by Bansal and Pindera (2003). This technique uses the volume-average of the different fields that define the material behavior, and imposes the boundary and continuity conditions in an average sense. The finite-volume theory has shown to be a well suitable method for elastic stress analysis, see references Cavalcante, Marques and Pindera (2007a,b and 2008) and Cavalcante and Pindera (2012a,b). The satisfaction of equilibrium equations at the subvolume level, concomitant to kinematic and static continuities forced in a surface-average sense between common interfaces of adjacent subvolumes, are features that distinguish the FVT from the FEM.

The numerical instabilities mentioned before, especially the checkerboard effect, are related to the solution assumptions of the FEM. In fact, the FEM establishes the equilibrium and compatibility conditions through the nodes of the finite elements that compose the discretized analysis domain. In addition, the equilibrium equations are not satisfied at the element level, being only satisfied when a sufficiently fine-mesh is employed. On the other hand, the finite-volume theory always satisfies the equilibrium equations at the subvolume level, and the kinematic and static compatibility conditions are established in an average-sense between common interfaces of adjacent subvolumes. Thus, in the finite-volume theory, the connections between subvolumes occur through the subvolume faces, as expected from a continuum mechanics point of view. At the same time, this is not observed in the displacement formulation of the finite-element method, where the connections between adjacent elements occur through the nodes, resulting in optimum topologies with checkerboard pattern.

## TOPOLOGY OPTIMIZATION PROBLEM

A topology optimization problem based on the power law approach, where the objective is to minimize the structural compliance function, can be expressed as

$$\begin{cases} \min c(\boldsymbol{\rho}) = \sum_{e=1}^{N} (\rho_e)^p \boldsymbol{d_e}^T \boldsymbol{K_e^0} \boldsymbol{d_e} \\ \text{subject to:} \\ \quad \frac{V(\boldsymbol{\rho})}{\bar{V}} = f \\ \quad 0 < \rho_{min} \leq \rho_e \leq 1 \end{cases} \tag{1}$$

where $V(\boldsymbol{\rho})$ and $\bar{V}$ are the material and reference domain volumes, respectively, $\boldsymbol{d_e}$ is the local displacement vector, $\boldsymbol{K_e^0}$ is the local stiffness matrix of the element $e$, $\boldsymbol{\rho}$ is the vector containing the relative densities of all elements, $p$ is the penalty factor, $f$ is the prescribed volume fraction, $\rho_{min}$ is the minimum relative density (different of zero to avoid singularity), $\rho_e$ is the relative density related to the element $e$ and $N$ is the total number of elements of the discretized analysis domain.

The topology optimization problem, shown in Eq. (1), can be solved by different approaches, however, for simplicity, it is usually employed the Optimality Criteria (OC) method. Following Araujo (2018), a heuristic update scheme for relative densities can be described as

$$\rho_e^{k+1} = \begin{cases} \max(\rho_{min}, \rho_e - m), \\ \quad \text{if } \rho_e^k B_e^\eta \leq \max(\rho_{min}, \rho_e - m) \\ \rho_e^k B_e^\eta, \\ \quad \text{if } \max(\rho_{min}, \rho_e - m) < \rho_e^k B_e^\eta < \min(1, \rho_e + m) \\ \min(1, \rho_e + m), \\ \quad \text{if } \min(1, \rho_e + m) \leq \rho_e^k B_e^\eta \end{cases} \tag{2}$$

where $k$ is the iteration index, $m$ is a positive move-limit, $\eta$ is a damping coefficient and $B_e$ is an expression given by

$$B_e = \frac{-\frac{\partial c}{\partial \rho_e}}{\lambda \frac{\partial f}{\partial \rho_e}} \tag{3}$$

where $\lambda$ is a Lagrangian multiplier for volume constraint and is determined using a bisection method.

## FINITE-VOLUME THEORY

An alternative technique to the FEM is presented by Aboudi et al. (1999) and it was originally denominated as the higher-order theory. According to Cavalcante (2006), this technique employs the volume average of the different fields that define the material behavior and imposes boundary and continuity conditions between adjacent subvolumes in a surface-averaged sense. Also, the FVT suggests a simplification to the higher-order theory by substituting the volume average of the displacement and stress fields for surface-averaged quantities associated to each interface of the subvolumes. Besides, this theory presents some similarities to the finite volume method employed in fluids mechanics

and presented in Versteeg and Malalasekera (1995), implying in the denomination of finite-volume theory for this new approach.

The first researches in FVT are dated from the year of 2002. The first article to suggest a simplification in the higher-order theory was Bansal and Pindera (2003), followed by Cavalcante (2006) and Cavalcante, Marques e Pindera (2007a,b), which contributed with a bidimensional parametric formulation, more appropriate for the thermoelastic analysis of structures with curved contours. The generalization of the FVT firstly appeared in Cavalcante and Pindera (2012a,b), where the surface-averaged rotations and curvatures are incorporated to the analysis of rectangular domains discretized into rectangular subvolumes.

Basically, Cavalcante and Pindera (2012a,b) generalized the FVT by adding higher-order terms to the incomplete quadratic representation of the displacement field, originally developed by Bansal and Pindera (2003). The generalization is accomplished by adding systematically different orders to the zeroth order FVT, which corresponds to the original version presented in Bansal and Pindera (2003). Each order corresponds to an increase in the displacement field complexity, followed by the addition of kinematic quantities evaluated in an average sense at the subvolume's faces and based on considerations of the elasticity theory, which introduces mechanic significance to the problem (Cavalcante and Pindera, 2012a). Thus, the first order FVT incorporates the rotations to the original version, while the second order FVT incorporates rotations and curvatures.

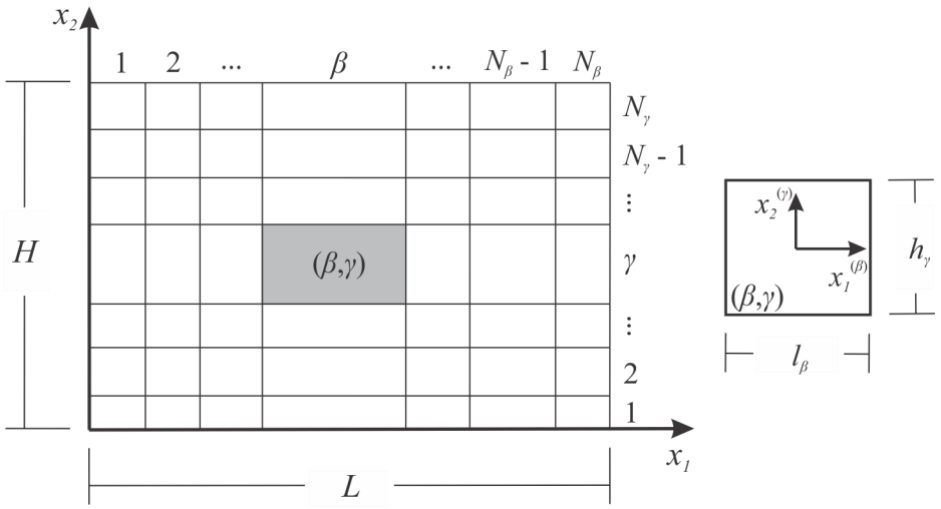


**Figure 1 – Analysis domain discretization and global coordinate system (left) and subvolume and local coordinate system (right).**

## Generalized formulation of the finite-volume theory for solid mechanics' analysis

Figure 1 shows the adopted rectangular domain in $x_1 - x_2$ plane with $0 \leq x_1 \leq L$ and $0 \leq x_2 \leq H$, which is discretized in $N_\beta$ horizontal subvolumes and $N_\gamma$ vertical subvolumes. The subvolume dimensions are $l_\beta$ and $h_\gamma$ (for $\beta = 1, \ldots, N_\beta$ and $\gamma = 1, \ldots, N_\gamma$ over the axis $x_1$ and $x_2$, respectively. Thus, following Cavalcante and Pindera (2012a), the displacement field of a $(\beta, \gamma)$ subvolume can be approximated by quadratic polynomials expressed in function of local coordinates inside each subvolume, as follows

$$\begin{aligned} u_i^{(\beta,\gamma)} = {} & W_{i(00)}^{(\beta,\gamma)} + x_1^{(\beta)} W_{i(10)}^{(\beta,\gamma)} + x_2^{(\gamma)} W_{i(01)}^{(\beta,\gamma)} + x_1^{(\beta)} x_2^{(\gamma)} W_{i(11)}^{(\beta,\gamma)} + \frac{1}{2}\left(3{x_1^{(\beta)}}^2 - \frac{l_\beta^2}{4}\right) W_{i(20)}^{(\beta,\gamma)} \\ & + \frac{1}{2}\left(3{x_2^{(\gamma)}}^2 - \frac{h_\gamma^2}{4}\right) W_{i(02)}^{(\beta,\gamma)} + \frac{1}{2}\left(3{x_1^{(\beta)}}^2 - \frac{l_\beta^2}{4}\right) x_2^{(\gamma)} W_{i(21)}^{(\beta,\gamma)} \\ & + \frac{1}{2}\left(3{x_2^{(\gamma)}}^2 - \frac{h_\gamma^2}{4}\right) x_1^{(\beta)} W_{i(12)}^{(\beta,\gamma)} + \frac{1}{4}\left(3{x_1^{(\beta)}}^2 - \frac{l_\beta^2}{4}\right)\left(3{x_2^{(\gamma)}}^2 - \frac{h_\gamma^2}{4}\right) W_{i(22)}^{(\beta,\gamma)} \end{aligned} \tag{4}$$

where $i = 1,2$ and $W_{i(mn)}^{(\beta,\gamma)}$ are unknown coefficients of the displacement field. Each coefficient can be expressed as a function of the following physical quantities: displacements, rotations and curvatures evaluated in an average-sense at the subvolume's faces.

### *Kinematic Variables in a Surface-Averaged Sense*

The surface-averaged displacement components are evaluated by the following expressions:

$$\bar{u}_i^{(1,3)} = \frac{1}{l_\beta}\int_{-l_\beta/2}^{l_\beta/2} u_i\left(x_1^{(\beta)}, \mp\frac{h_\gamma}{2}\right) dx_1^{(\beta)} \tag{5}$$

$$\bar{u}_i^{(2,4)} = \frac{1}{h_\gamma}\int_{-h_\gamma/2}^{h_\gamma/2} u_i\left(\pm\frac{l_\beta}{2}, x_2^{(\gamma)}\right) dx_2^{(\gamma)} \tag{6}$$

where the superscript indicates the subvolume face number, as illustrated in Figure 2. At the same time, the surface-averaged rotation components can be defined as

$$\bar{\theta}_{21}^{(1,3)} = \frac{1}{l_\beta}\int_{-l_\beta/2}^{l_\beta/2} \frac{\partial u_2\left(x_1^{(\beta)}, \mp\frac{h_\gamma}{2}\right)}{\partial x_1^{(\beta)}} dx_1^{(\beta)} \tag{7}$$

$$\bar{\theta}_{12}^{(2,4)} = \frac{1}{h_\gamma}\int_{-h_\gamma/2}^{h_\gamma/2} \frac{\partial u_1\left(\pm\frac{l_\beta}{2}, x_2^{(\gamma)}\right)}{\partial x_2^{(\gamma)}} dx_2^{(\gamma)} \tag{8}$$

and the surface-averaged curvature components can be defined as

$$\bar{\kappa}_{21}^{(1,3)} = \frac{1}{l_\beta}\int_{-l_\beta/2}^{l_\beta/2} \frac{\partial^2 u_2\left(x_1^{(\beta)}, \mp\frac{h_\gamma}{2}\right)}{\partial x_1^{2(\beta)}} dx_1^{(\beta)} \tag{9}$$

$$\bar{\kappa}_{12}^{(2,4)} = \frac{1}{h_\gamma}\int_{-h_\gamma/2}^{h_\gamma/2} \frac{\partial^2 u_1\left(\pm\frac{l_\beta}{2}, x_2^{(\gamma)}\right)}{\partial x_2^{2(\gamma)}} dx_2^{(\gamma)} \tag{10}$$

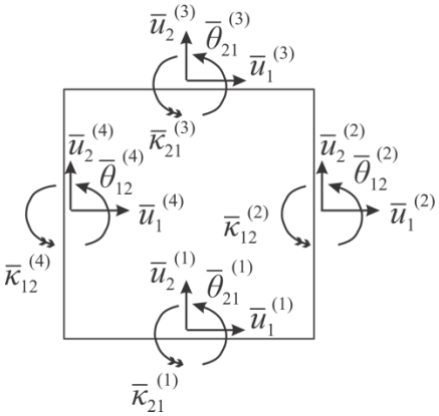


**Figure 2 – Kinematic quantities in surface average-sense of the subvolume $(\beta, \gamma)$.**

The next step refers to the compatibilization of kinematic variables in surface-averaged sense, which is motivated by the establishing of continuity conditions through the faces between adjacent subvolumes (Cavalcante and Pindera, 2012a). Thus, the kinematic compatibilization between the third and first faces of each adjacent subvolumes on the discretized structure can be defined as

$$\bar{u}_i^{(3)}\Big|^{(\beta,\gamma)} = \bar{u}_i^{(1)}\Big|^{(\beta,\gamma)} \tag{11}$$

$$\theta_{21}^{(3)}\Big|^{(\beta,\gamma)} = \theta_{12}^{(1)}\Big|^{(\beta,\gamma)} \tag{12}$$

$$\kappa_{21}^{(3)}\Big|^{(\beta,\gamma)} = \kappa_{12}^{(1)}\Big|^{(\beta,\gamma)} \tag{13}$$

Similarly, the displacement field must be also compatibilized between the fourth and second faces of adjacent subvolumes.

By substituting Eq. (4) in Eqs. (5), (6), (7), (8), (9) and (10), 16 expressions are obtained for displacements, rotations and curvatures in a surface-averaged sense. These expressions can be organized in matrix notation as follows:

$$\begin{bmatrix}\bar{\mathbf{u}}^{(\beta,\gamma)}\\ \bar{\boldsymbol{\theta}}^{(\beta,\gamma)}\\ \bar{\boldsymbol{\kappa}}^{(\beta,\gamma)}\end{bmatrix} = \mathbf{A}_{(16\times16)}^{(\beta,\gamma)}\begin{bmatrix}\mathbf{W}^{(\beta,\gamma)}\\ \mathbf{W}_{\nabla}^{(\beta,\gamma)}\\ \mathbf{W}_{\nabla^2}^{(\beta,\gamma)}\end{bmatrix} + \mathbf{a}_{(16\times2)}^{(\beta,\gamma)}\mathbf{W}_{(00)}^{(\beta,\gamma)} \tag{14}$$

where $\bar{\mathbf{u}}^{(\beta,\gamma)}$ is the local vector composed by the surface-averaged displacements in the subvolume $(\beta,\gamma)$, $\bar{\boldsymbol{\theta}}^{(\beta,\gamma)}$ is the local vector formed by the surface-averaged rotations in the subvolume $(\beta,\gamma)$, $\bar{\boldsymbol{\kappa}}^{(\beta,\gamma)}$ is the local vector composed by the surface-averaged curvatures in the subvolume $(\beta,\gamma)$, $\mathbf{W}^{(\beta,\gamma)} = \left[W_{1(10)}^{(\beta,\gamma)}, W_{1(01)}^{(\beta,\gamma)}, W_{1(20)}^{(\beta,\gamma)}, W_{1(02)}^{(\beta,\gamma)}, W_{2(10)}^{(\beta,\gamma)}, W_{2(01)}^{(\beta,\gamma)}, W_{2(20)}^{(\beta,\gamma)}, W_{2(02)}^{(\beta,\gamma)}\right]^T$, $\mathbf{W}_{\nabla^2}^{(\beta,\gamma)} = \left[W_{1(11)}^{(\beta,\gamma)}, W_{2(11)}^{(\beta,\gamma)}, W_{1(21)}^{(\beta,\gamma)}, W_{2(12)}^{(\beta,\gamma)}\right]^T$, $\mathbf{W}_{(00)}^{(\beta,\gamma)} = \left[W_{1(12)}^{(\beta,\gamma)}, W_{2(21)}^{(\beta,\gamma)}, W_{1(22)}^{(\beta,\gamma)}, W_{2(22)}^{(\beta,\gamma)}\right]^T$ and $\mathbf{W}_{(00)}^{(\beta,\gamma)} = \left[W_{1(00)}^{(\beta,\gamma)}, W_{2(00)}^{(\beta,\gamma)}\right]^T$. $\mathbf{A}_{(16\times16)}^{(\beta,\gamma)}$ and $\mathbf{a}_{(16\times2)}^{(\beta,\gamma)}$ are matrixes that depends on the geometric characteristics of the subvolume $(\beta,\gamma)$.

### *Static Variables in a Surface Average-sense*

The static variables evaluated in a surface-averaged sense can be expressed by

$$\bar{t}_i^{(1,3)} = \mp\frac{1}{l_\beta}\int_{-l_\beta/2}^{l_\beta/2}\sigma_{2i}\left(x_1^{(\beta)}, \mp\frac{h_\gamma}{2}\right)dx_1^{(\beta)} \tag{15}$$

$$\bar{t}_i^{(2,4)} = \pm\frac{1}{h_\gamma}\int_{-h_\gamma/2}^{h_\gamma/2}\sigma_{1i}\left(\pm\frac{l_\beta}{2}, x_2^{(\gamma)}\right)dx_2^{(\gamma)} \tag{16}$$

$$\bar{t}_{2/1}^{(1,3)} = \mp\frac{1}{l_\beta}\int_{-l_\beta/2}^{l_\beta/2}\frac{\partial\sigma_{22}\left(x_1^{(\beta)}, \mp\frac{h_\gamma}{2}\right)}{\partial x_1^{(\beta)}}dx_1^{(\beta)} \tag{17}$$

$$\bar{t}_{1/2}^{(2,4)} = \pm\frac{1}{h_\gamma}\int_{-h_\gamma/2}^{h_\gamma/2}\frac{\partial\sigma_{11}\left(\pm\frac{l_\beta}{2}, x_2^{(\gamma)}\right)}{\partial x_2^{(\gamma)}}dx_2^{(\gamma)} \tag{18}$$

$$\bar{t}_{2/11}^{(1,3)} = \mp\frac{1}{l_\beta}\int_{-l_\beta/2}^{l_\beta/2}\frac{\partial^2\sigma_{22}\left(x_1^{(\beta)}, \mp\frac{h_\gamma}{2}\right)}{\partial x_1^{2(\beta)}}dx_1^{(\beta)} \tag{19}$$

$$\bar{t}_{1/22}^{(2,4)} = \pm\frac{1}{h_\gamma}\int_{-h_\gamma/2}^{h_\gamma/2}\frac{\partial^2\sigma_{11}\left(\pm\frac{l_\beta}{2}, x_2^{(\gamma)}\right)}{\partial x_2^{2(\gamma)}}dx_2^{(\gamma)} \tag{20}$$

While the continuity conditions between the third and first faces of adjacent subvolumes can be stated as

$$t_i^{(3)}\Big|^{(\beta,\gamma)} - t_i^{(1)}\Big|^{(\beta,\gamma+1)} = 0 \tag{21}$$

$$t_{2/1}^{(3)}\Big|^{(\beta,\gamma)} - t_{2/1}^{(1)}\Big|^{(\beta,\gamma+1)} = 0 \tag{22}$$

$$t_{2/11}^{(3)}\Big|^{(\beta,\gamma)} - t_{2/11}^{(1)}\Big|^{(\beta,\gamma+1)} = 0 \tag{23}$$

Considering a linear elastic material, the generalized Hooke`s law for the subvolume $(\beta,\gamma)$ can be expressed as

$$\sigma_{ij}^{(\beta,\gamma)} = C_{ijkl}^{(\beta,\gamma)}\varepsilon_{kl}^{(\beta,\gamma)} \tag{24}$$

where $C_{ijkl}^{(\beta,\gamma)}$ are the material stiffness tensor components which fills the subvolume $(\beta,\gamma)$ and $\varepsilon_{kl}^{(\beta,\gamma)}$ are the strain tensor components. Applying the assumptions of the elasticity theory for isotropic materials and substituting the Eq. (4) in Eqs. (15), (16), (17), (18), (19) and (20), we can get 16 expressions in terms of the unknown coefficients of the displacement field. These expressions can be organized in matrix notation as follows

$$\begin{bmatrix}\bar{\mathbf{t}}^{(\beta,\gamma)}\\ \bar{\mathbf{t}}_\nabla^{(\beta,\gamma)}\\ \bar{\mathbf{t}}_{\nabla^2}^{(\beta,\gamma)}\end{bmatrix} = \mathbf{B}_{(16\times16)}^{(\beta,\gamma)}\begin{bmatrix}\mathbf{W}^{(\beta,\gamma)}\\ \mathbf{W}_\nabla^{(\beta,\gamma)}\\ \mathbf{W}_{\nabla^2}^{(\beta,\gamma)}\end{bmatrix} \tag{25}$$

where $\bar{\mathbf{t}}^{(\beta,\gamma)}$ is the local vector formed by surface-averaged tractions acting on the faces of the subvolume $(\beta,\gamma)$, $\bar{\mathbf{t}}_\nabla^{(\beta,\gamma)}$ is the local vector containing the surface-averaged first derivatives of the normal traction components acting on the faces of the subvolume $(\beta,\gamma)$ and $\bar{\mathbf{t}}_{\nabla^2}^{(\beta,\gamma)}$ is the local vector containing the surface-averaged second derivatives of the normal traction components acting on the faces of the subvolume $(\beta,\gamma)$. $\mathbf{B}_{(16\times16)}^{(\beta,\gamma)}$ is a matrix that depends on the geometric characteristics and the material properties of the subvolume $(\beta,\gamma)$.

### *Local Equilibrium at the Subvolume Level*

In the absence of body forces, the satisfaction of equilibrium conditions can be achieved by the following expression:

$$\sum_{p=1}^{4} \bar{\mathbf{t}}_{(p)}^{(\beta,\gamma)} L_p^{(\beta,\gamma)} = \mathbf{0} \tag{26}$$

where $L_1^{(\beta,\gamma)} = l_\beta$, $L_2^{(\beta,\gamma)} = h_\gamma$, $L_3^{(\beta,\gamma)} = l_\beta$ and $L_4^{(\beta,\gamma)} = h_\gamma$ are the faces' lengths of the subvolume $(\beta,\gamma)$ and $\bar{\mathbf{t}}_{(p)}^{(\beta,\gamma)}$ can be written as

$$\bar{\mathbf{t}}_{(p)}^{(\beta,\gamma)} = \mathbf{B}_{(2\times16)}^{(\beta,\gamma,p)} \left(\mathbf{A}_{16\times16}^{(\beta,\gamma)}\right)^{-1} \bar{\mathbf{u}}^{(\beta,\gamma)} - \mathbf{B}_{(2\times16)}^{(\beta,\gamma,p)} \left(\mathbf{A}_{16\times16}^{(\beta,\gamma)}\right)^{-1} \mathbf{a}_{(16\times2)}^{(\beta,\gamma)} \mathbf{W}_{(00)}^{(\beta,\gamma)} \tag{27}$$

where $\mathbf{B}_{(2\times16)}^{(\beta,\gamma,p)}$ are submatrices that select the components of $\mathbf{B}_{(16\times16)}^{(\beta,\gamma)}$, which are related only to the surface-averaged tractions acting on the face $p$ of the subvolume $(\beta,\gamma)$.

Substituting Eqs. (14) and (25) in Eq. (27), then substituting this result in Eq. (26), follows

$$\left(\sum_{p=1}^{4} \mathbf{B}_{(2\times16)}^{(\beta,\gamma,p)} L_p^{(\beta,\gamma)}\right) \left(\mathbf{A}_{(16\times16)}^{(\beta,\gamma)}\right)^{-1} \begin{bmatrix} \bar{\mathbf{u}}^{(\beta,\gamma)} \\ \bar{\boldsymbol{\theta}}^{(\beta,\gamma)} \\ \bar{\boldsymbol{\kappa}}^{(\beta,\gamma)} \end{bmatrix} = \left(\sum_{p=1}^{4} \mathbf{B}_{(2\times16)}^{(\beta,\gamma,p)} L_p^{(\beta,\gamma)}\right) \left(\mathbf{A}_{(16\times16)}^{(\beta,\gamma)}\right)^{-1} \mathbf{a}_{(16\times2)}^{(\beta,\gamma)} \mathbf{W}_{(00)}^{(\beta,\gamma)} \tag{28}$$

### *Local Stiffness Matrix*

From Eq. (28), the vector $\mathbf{W}_{(00)}^{(\beta,\gamma)}$ can be evaluated as follows

$$\mathbf{W}_{(00)}^{(\beta,\gamma)} = \bar{\mathbf{a}}_{(2\times16)}^{(\beta,\gamma)} \begin{bmatrix} \bar{\mathbf{u}}^{(\beta,\gamma)} \\ \bar{\boldsymbol{\theta}}^{(\beta,\gamma)} \\ \bar{\boldsymbol{\kappa}}^{(\beta,\gamma)} \end{bmatrix} \tag{29}$$

where

$$\bar{\mathbf{a}}_{(2\times16)}^{(\beta,\gamma)} = \left[\left(\sum_{p=1}^{4} \mathbf{B}_{(2\times16)}^{(\beta,\gamma,p)} L_p^{(q)}\right) \left(\mathbf{A}_{(16\times16)}^{(\beta,\gamma)}\right)^{-1} \mathbf{a}_{(16\times2)}^{(\beta,\gamma)}\right]^{-1} \left(\sum_{p=1}^{4} \mathbf{B}_{(2\times16)}^{(\beta,\gamma,p)} L_p^{(\beta,\gamma)}\right) \left(\mathbf{A}_{(16\times16)}^{(\beta,\gamma)}\right)^{-1} \tag{30}$$

Inserting Eq. (29) in Eq. (4), the result can be written as

$$\begin{bmatrix} \mathbf{W}^{(\beta,\gamma)} \\ \mathbf{W}_{\nabla}^{(\beta,\gamma)} \\ \mathbf{W}_{\nabla^2}^{(\beta,\gamma)} \end{bmatrix} = \bar{\mathbf{A}}_{(16\times16)}^{(\beta,\gamma)} \begin{bmatrix} \bar{\mathbf{u}}^{(\beta,\gamma)} \\ \bar{\boldsymbol{\theta}}^{(\beta,\gamma)} \\ \bar{\boldsymbol{\kappa}}^{(\beta,\gamma)} \end{bmatrix} \tag{31}$$

where

$$\bar{\mathbf{A}}_{(16\times16)}^{(\beta,\gamma)} = \left(\mathbf{A}_{(16\times16)}^{(\beta,\gamma)}\right)^{-1} - \left(\mathbf{A}_{(16\times16)}^{(\beta,\gamma)}\right)^{-1} \mathbf{a}_{(16\times2)}^{(\beta,\gamma)} \bar{\mathbf{a}}_{(2\times16)}^{(\beta,\gamma)} \tag{32}$$

Substituting Eqs. (29) and (31) in Eq. (25), we have the following linear system of equations that relates the static and kinematic variables:

$$\begin{bmatrix} \bar{\mathbf{t}}^{(\beta,\gamma)} \\ \bar{\mathbf{t}}_{\nabla}^{(\beta,\gamma)} \\ \bar{\mathbf{t}}_{\nabla^2}^{(\beta,\gamma)} \end{bmatrix} = \mathbf{K}_{(16\times16)}^{(\beta,\gamma)} \begin{bmatrix} \bar{\mathbf{u}}^{(\beta,\gamma)} \\ \bar{\boldsymbol{\theta}}^{(\beta,\gamma)} \\ \bar{\boldsymbol{\kappa}}^{(\beta,\gamma)} \end{bmatrix} \tag{33}$$

where $\mathbf{K}_{(16\times16)}^{(\beta,\gamma)} = \mathbf{B}_{(16\times16)}^{(\beta,\gamma)} \bar{\mathbf{A}}_{(16\times16)}^{(\beta,\gamma)}$ is the local stiffness matrix of the subvolume $(\beta,\gamma)$.

### *Global Stiffness Matrix*

The global stiffness matrix of the structure is assembled considering the individual contribution of each subvolume of the discretized domain. Considering a structure discretized in $N_\beta$ by $N_\gamma$ subvolumes, as there are four degrees of freedom in each face, then the number of degrees of freedom is given by $N_{gl} = 4N_\beta\left(N_\gamma + 1\right) + 4\left(N_\beta + 1\right)N_\gamma$. Based on the kinematic and static continuity conditions, the expression that defines the global system of equations can be written as

$$\mathbf{T}_{(N_{gl}\times1)} = \mathbf{K}_{(N_{gl}\times N_{gl})} \mathbf{U}_{(N_{gl}\times1)} \tag{34}$$

where $\mathbf{U}_{(N_{gl}\times 1)}$ and $\mathbf{T}_{(N_{gl}\times 1)}$ are the global surface-averaged kinematic and static vectors of the structure, respectively, and the global stiffness matrix can be obtained as follows

$$\mathbf{K}_{(N_{gl}\times N_{gl})} = \sum_{\gamma=1}^{N_\gamma}\sum_{\beta=1}^{N_\beta}\left[\left(\mathbf{L}_{(16\times N_{gl})}^{(\beta,\gamma)}\right)^T \mathbf{K}_{(16\times 16)}^{(\beta,\gamma)}\mathbf{L}_{(16\times N_{gl})}^{(\beta,\gamma)}\right] \tag{35}$$

where $\mathbf{L}_{(16\times N_{gl})}^{(\beta,\gamma)}$ is the kinematic and static incidence matrix of the subvolume $(\beta,\gamma)$. The formulations for lower orders can be obtained uncoupling the curvatures, in the case of the first order finite-volume theory, and curvatures and rotations, in the case of the zeroth order finite-volume theory.

## Evaluation of the Compliance Function for the Generalized Finite-Volume Theory

Since the first work, presented by Bendsøe and Kikuchi (1988), an important part of the advances in topology optimization has been made through methodologies based on minimization of structural elastic strain energy related to the work done by external forces (Collet, Bruggi and Duysinx, 2017). This problem is usually called as structural compliance minimization, or maximization of the global stiffness. The compliance function can be defined as twice the strain energy occasioned by the displacement field $\mathbf{u}$:

$$c(\mathbf{u},\boldsymbol{\rho}) = 2U(\mathbf{u},\boldsymbol{\rho}) = \iiint_\Omega 2\bar{U}(\mathbf{u},\boldsymbol{\rho})\,d\Omega = \iiint_\Omega \sigma_{ij}(\mathbf{u},\boldsymbol{\rho})\varepsilon_{ij}(\mathbf{u},\boldsymbol{\rho})\,d\Omega = \iiint_\Omega \frac{1}{2}C_{ijkl}(\boldsymbol{\rho})\varepsilon_{kl}(\mathbf{u})\varepsilon_{ij}(\mathbf{u})\,d\Omega \tag{36}$$

where $c(\mathbf{u},\boldsymbol{\rho})$ is the compliance function, $U(\mathbf{u},\boldsymbol{\rho})$ is the strain energy, $\bar{U}(\mathbf{u},\boldsymbol{\rho})$ is the specific strain energy, $\sigma_{ij}(\mathbf{u},\boldsymbol{\rho})$ is the stress tensor, $\varepsilon_{ij}(\mathbf{u})$ is the strain tensor, $C_{ijkl}(\boldsymbol{\rho})$ is the material stiffness tensor, $\Omega$ is the analysis domain and $\boldsymbol{\rho}$ is the relative density field.

For the finite element method based on trilateral linear elements and the zeroth order finite-volume theory is valid the equivalence between the total strain energy and the work done by the external forces, as shown in Eq. (36), once the differential equilibrium equations are satisfied pointwise inside the element or subvolume. However, this consideration is extended to all other formulations with the intention to simplify the evaluation of the objective function, so, the following assumption is adopted to the definition of the compliance function in this article:

$$c(\mathbf{u},\boldsymbol{\rho}) = 2U(\mathbf{u},\boldsymbol{\rho}) = 2W(\mathbf{u},\boldsymbol{\rho}) = \iint_{S_\sigma} t_i u_i\,dS \tag{37}$$

where $W(\mathbf{u},\boldsymbol{\rho})$ is the work done by the external forces, $t_i$ is the traction vector acting on the boundary, $u_i$ is the displacement vector and $S_\sigma$ is the external surface subjeted to external loadings or with the traction free condition, being the complementary to the external surface with displacement restrictions.

As a result, the compliance function for the generalized finite-volume theory can be evaluated as follows

$$c(\mathbf{U},\boldsymbol{\theta},\boldsymbol{\kappa},\boldsymbol{\rho}) = \sum_{\gamma=1}^{N_\gamma}\sum_{\beta=1}^{N_\beta}\left(\rho_{(\beta,\gamma)}\right)^p\left[\mathbf{L}_{(0)}^{(\beta,\gamma)}\mathbf{t}^{(\beta,\gamma)}\right]^T\mathbf{u}^{(\beta,\gamma)} + \sum_{\gamma=1}^{N_\gamma}\sum_{\beta=1}^{N_\beta}\left(\rho_{(\beta,\gamma)}\right)^p\left[\mathbf{L}_{(1)}^{(\beta,\gamma)}\mathbf{t}_\nabla^{(\beta,\gamma)}\right]^T\boldsymbol{\theta}^{(\beta,\gamma)} + \sum_{\gamma=1}^{N_\gamma}\sum_{\beta=1}^{N_\beta}\left(\rho_{(\beta,\gamma)}\right)^p\left[\mathbf{L}_{(2)}^{(\beta,\gamma)}\mathbf{t}_{\nabla^2}^{(\beta,\gamma)}\right]^T\boldsymbol{\kappa}^{(\beta,\gamma)} \tag{38}$$

where $\mathbf{U}$ is the global vector containing the surface-average displacements, $\boldsymbol{\theta}$ is the global vector containing the surface-average rotations, $\boldsymbol{\kappa}$ is the global vector containing the surface-averaged curvatures, $\boldsymbol{\rho}$ is the vector containing the relative densities of all subvolumes, $\rho_{(\beta,\gamma)}$ is the relative density associated with the subvolume $(\beta,\gamma)$ and $\mathbf{L}_{(.)}^{(\beta,\gamma)}$ are matrixes that dependents on the subvolume geometry. Finally, the objective function sensitivity analysis can be evaluated by the compliance function gradient as follows

$$\frac{\partial c}{\partial \rho_{(\beta,\gamma)}}\left(\mathbf{u}^{(\beta,\gamma)},\boldsymbol{\theta}^{(\beta,\gamma)},\boldsymbol{\kappa}^{(\beta,\gamma)},\rho_{(\beta,\gamma)}\right) = -p\left(\rho_{(\beta,\gamma)}\right)^{p-1}\left\{\left[\mathbf{L}_{(0)}^{(\beta,\gamma)}\mathbf{t}^{(\beta,\gamma)}\right]^T\mathbf{u}^{(\beta,\gamma)} + \left[\mathbf{L}_{(1)}^{(\beta,\gamma)}\mathbf{t}_\nabla^{(\beta,\gamma)}\right]^T\boldsymbol{\theta}^{(\beta,\gamma)} + \left[\mathbf{L}_{(2)}^{(\beta,\gamma)}\mathbf{t}_{\nabla^2}^{(\beta,\gamma)}\right]^T\boldsymbol{\kappa}^{(\beta,\gamma)}\right\} \tag{39}$$

The compliance functions and its sensitivities for lower order formulations of the generalized finite-volume theory can be obtained by uncoupling curvatures (for the first order FVT), and curvatures and rotations (for the zeroth order FVT).

## NUMERICAL RESULTS

The *Messerschmitt-Bölkow-Blom* (MBB) beam, shown in Figure 3, is a classical problem in topology optimization, so, here, this example is employed for efficiency comparison between the three versions of the generalized finite-volume theory and the element Q4 (rectangular bilinear element with four nodes) of the finite-element method. In the model conception, consistent units for the physical and geometric parameters are adopted. In the absence of filtering techniques and image processing, the following numerical aspects are investigated: number of iterations, processing

time and convergence. In order to avoid local minima issues, the continuation scheme of penalization, where the penalty factor increases gradually ($\Delta p = 0.5$) from $p = 1$ to $p = 4$, has been adopted, as suggested by Talischi et al. (2012). Taking advantage of the symmetry, only half of the analysis domain is analyzed, employing boundary conditions that reflect this symmetry.

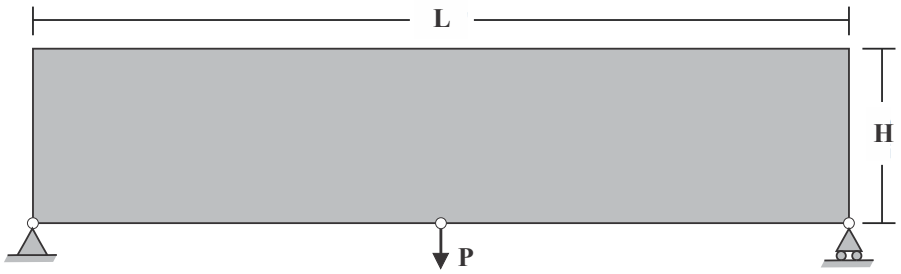


**Figure 3 – *Messerschmitt-Bölkow-Blom* (MBB) beam.**

As convergence criterion, it is adopted the maximum tolerance for the change in relative densities of successive steps, which was set as 1%. The damping factor $\eta$ varies for different approaches, with the goal to obtain the minimum value that avoids numerical divergence caused by the oscillatory phenomenon. The computational environment in terms of programming language and machine can be described as: MatLab R2016a (64-bits)/Intel® Core™ i5-4200U CPU @ 1.60 GHz 2.30 GHz/8.0 GB RAM/64-bits.

The proposed optimization problem consists on finding the lower value for the compliance function of a structure defined in Figure 3, with a restriction of 50% of the total volume. Figure 4 presents the optimum topologies obtained for the approaches applying the zeroth, first and second orders FVT (FVT-0$^{th}$, FVT-1$^{st}$ and FVT-2$^{nd}$, respectively), and the finite-element Q4. In addition, the adopted mesh is 240x40, which gives a total of 9600 square subvolumes or elements.

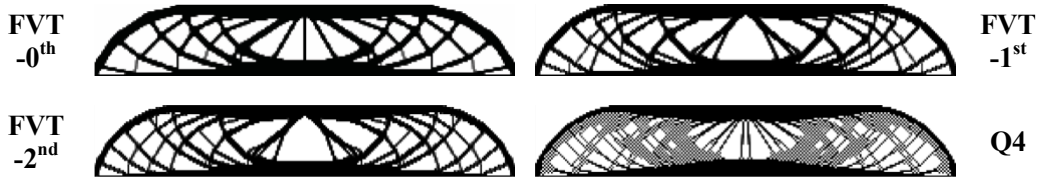


**Figure 4 – Optimum topologies obtained for MBB beam analysis and a mesh size of 240x40.**

In Figure 4, the optimum topologies obtained with the FVT approaches are checkerboard-free. On the other hand, the results obtained by finite-element Q4, without filtering techniques, usually leads to optimum topologies with the checkerboard pattern effect. According to Díaz and Sigmund (1995), the arising of the checkerboard pattern in an optimum topology is due to the approximations from the FEM, which leads to structures artificially rigid. Basically, the FEM forces the satisfaction of equilibrium equations and compatibility conditions through the nodes, while the FVT satisfies these features in a more likely continuum mechanics point of view.

**Table 1 – Convergence study for MBB beam of 240x40 mesh size.**

| Analysis | NDOF | Number of iterations | Processing time (seconds) | Damping factor |
|---|---|---|---|---|
| FVT-0$^{th}$ | 19520 | 464 | 2366.45 | 1/2.6 |
| FVT-1$^{st}$ | 29280 | 639 | 7735.88 | 1/11.3 |
| FVT-2$^{nd}$ | 39040 | 722 | 13206.05 | 1/11.2 |
| Q4 | 9922 | 726 | 2273.12 | 1/2.5 |

Table 1 shows the number of iterations, processing time, number of degrees of freedom (NDOF) and adopted damping factor. Basically, the number of iterations and computational cost are higher for the first and second order FVT, in comparison with the zeroth order version, which can be explained by the low values set up for the damping factor, besides the higher number of degrees of freedom. The finite-element Q4 presents the highest number of iterations, but the smallest computational cost, due the smallest number of degrees of freedom. The processing time in the zeroth order FVT is approximately the same observed for the approach based on the FEM. Basically, the FEM approach had convergence difficulties during the optimization process, what led to a higher number of iterations, affecting negatively the computational cost, besides the optimum topology with the checkerboard pattern.

The second example is the *Michell* Structure, shown in Figure 5. In the analysis of the proposed model, consistent units for the geometric and physical parameters are adopted. As in the previous example, the use of filtering or image processing are avoided, while the continued penalization scheme is adopted to avoid local minima, where the penalty

factor increases gradually ($\Delta p = 0.5$) from $p = 1$ to $p = 4$. In addition, different values are adopted for the damping factor, in order to avoid divergence caused by the oscillatory phenomenon on the employed approaches.

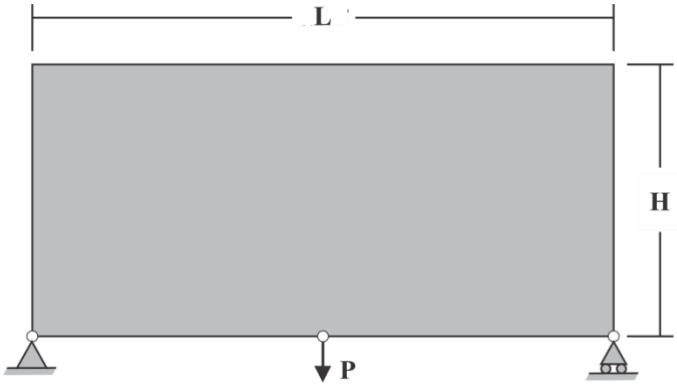


**Figure 5 – *Michell* structure.**

Here, the optimization problem consists on finding the lower value for compliance function of a structure that has the analysis domain and boundary conditions as shown in Figure 5, with a restriction of 40% of the total volume. Figure 6 shows the optimum topologies obtained for the approaches based on the zeroth, first and second orders FVT, and the finite-element Q4. The mesh size adopted is 160x80, which gives a total of 12800 square elements or subvolumes.

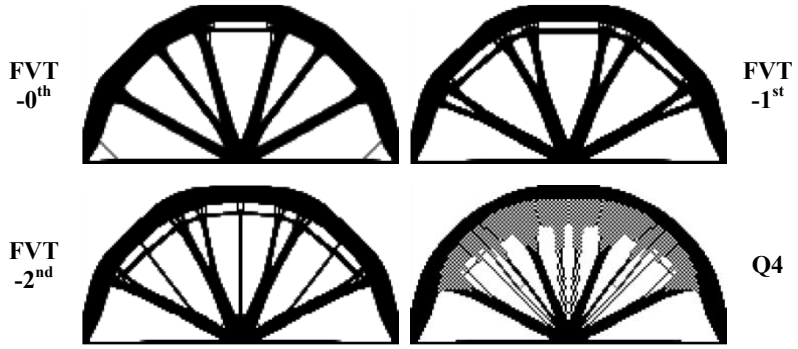


**Figure 6 – Optimum topologies obtained for *Michell* structure analysis with a mesh size of 160x80.**

As in the previous example, the optimum topologies obtained by the approaches based on FVT has shown to be checkerboard-free, while the approach based on the FEM has presented the checkerboard pattern effect in some parts of the structure. In fact, the checkerboard pattern effect is directly related to the displacement assumptions of the FEM. Basically, the satisfaction of equilibrium equations and compatibility conditions through the nodes cause the problem related to the checkerboard effect.

**Table 2 – Convergence study for *Michell* structure of 160x80 mesh size.**

| Analysis | NDOF | Number of iterations | Processing time (seconds) | Damping factor |
|---|---|---|---|---|
| FVT-0th | 25920 | 466 | 5383.16 | 1/2.6 |
| FVT-1st | 38880 | 657 | 14983.73 | 1/5 |
| FVT-2nd | 51840 | 750 | 24941.80 | 1/5.1 |
| Q4 | 13122 | 408 | 2322.04 | 1/2.6 |

Table 2 shows the number of iterations, the processing time, the number of degrees of freedom (NDOF) and the adopted damping factor for the analysis of a *Michell* structure with a mesh size of 160x80. In this case, the number of iterations has varied depending on the complexity of the adopted approach. Basically, it has increased as the NDOF increases and the damping factor decreases. Directly related to it, the computational cost has become higher as the number of iterations and the NDOF increase, once lower values for the damping factor makes the OC method algorithm to set small steps towards to the optimum design, and the NDOF defines the problem size. In this example, the computational cost for the zeroth order FVT is 2.3 times the same approach based on the FEM. The NDOF explains partially this difference in the processing time, because it defines the size of the global system of equations and the number of iterations was similar for this example.

## CONCLUDING REMARKS

The gradient-based topology optimization algorithms based on the FVT has shown to be efficient in the absence of filtering techniques. They are able to produce checkerboard-free optimum topologies. This efficiency is a result of the satisfaction of continuity conditions in a surface average-sense between adjacent subvolumes, which leads to connections through the interfaces among the subvolumes of the discretized analysis domain.

Despite the proven efficiency of the FVT to avoid checkerboard pattern in an optimum topology, this paper does not want to suggest the immediately substitution of the FEM in topology optimization algorithms, since there are several topology optimization techniques based on the FEM that have shown to be efficient as well, see Jang et al. (2003) and Pereira et al. (2010). In this paper, the FEM is employed as a validation source and to allow a comparative analysis of computational performance.

Based on the obtained results, the continuation of this investigation is justified by trying to explore the most different aspects of the FVT, especially in the case of heterogeneous materials with periodic microstructure, where the FVT technique has shown to be even more efficient.

## ACKNOWLEDGMENTS

The authors acknowledge the financial support provided by the Brazilian federal agency CNPq.

## REFERENCES

Araujo, M.V.O., 2018, “Teoria de Volumes Finitos Aplicada à Otimização Topológica de Estruturas Elásticas Contínuas”, Thesis (Master in Civil Engineering) – Federal University of Alagoas, Maceió, Brazil, 161 p.

Bansal, Y. and Pindera, M.J., 2003, “Efficient Reformulation of the Thermoelastic Higher-Order Theory for Functionally Graded Materials”, Journal of Thermal Stress, Vol. 26, No. 11-12, pp. 1055-1092.

Bendsøe, M.P. and Kikuchi, N., 1988, “Generating Optimal Topologies in Structural Design Using a Homogenization Method”, Computer Methods in Applied Mechanics and Engineering, Vol. 71, No. 2, pp. 197-224.

Bendsøe, M.P. and Sigmund, O., 2003, “Topology Optimization: Theory, Methods and Application”, Ed. Springer-Verlag, Berlin, Germany, 393 p.

Cavalcante, M.A.A., 2006, “Modelagem do Comportamento Termomecânico Transiente de Estruturas de Materiais Compósitos pela Teoria de Volumes Finitos”, Thesis (Master in Civil Engineering) – Federal University of Alagoas, Maceió, Brazil, 164 p.

Cavalcante, M.A.A., Marques, S.P. and Pindera, M.J., 2007a, “Parametric Formulation of the Finite-Volume Theory for Functionally Graded Materials – Part I: Analysis”, Journal of Applied Mechanics, Vol. 74, No. 5, pp. 935-945.

Cavalcante, M.A.A., Marques, S.P. and Pindera, M.J., 2007b, “Parametric Formulation of the Finite-Volume Theory for Functionally Graded Materials – Part II: Numerical Results”, Journal of Applied Mechanics, Vol. 74, No. 5, pp. 946-957.

Cavalcante, M.A.A., Marques, S.P. and Pindera, M.J., 2008, “Computational Aspects of the Parametric Finite-Volume Theory for Functionally Graded Materials”, Computational Material Science, Vol. 44, No. 2, pp. 422-438.

Cavalcante, M.A.A. and Pindera, M.J., 2012a, “Generalized Finite-Volume Theory for Elastic Stress Analysis in Solid Mechanics – Part I: Framework”, Journal of Applied Mechanics, Vol. 79, No. 5, pp. 051006.

Cavalcante, M.A.A. and Pindera, M.J., 2012b, “Generalized Finite-Volume Theory for Elastic Stress Analysis in Solid Mechanics – Part II: Results”, Journal of Applied Mechanics, Vol. 79, No. 5, pp. 051007.

Collet, M., Bruggi, M. and Duysinx, P., 2017, “Topology Optimization for Minimum Weight with Compliance and Simplified Nominal Stress Constraints for Fatigue Resistance”, Struct. and Multidisc. Optim., Vol. 55, pp. 839-855.

Díaz, A. and Sigmund, O., 1995, “Checkerboard Patterns in Layout Optimization”, Struct. and Multidisc. Optim., Vol. 10, No. 1, pp. 40-45.

Jang, G.W. et al., 2003, “Checkerboard-Free Topology Optimization using Non-Conforming Finite Elements”, International Journal for Numerical Methods in Engineering, Vol. 57, No. 12, pp. 1717-1735.

Pereira, A. et al., 2010, “Checkerboard-Free Topology Optimization Using Polygonal Finite Elements”, Mecánica Computacional, Vol. 29, No. 15, pp. 1525-1534.

Sigmund, O. and Petersson, J., 1998, “Numerical Instabilities in Topology Optimization: A Survey on Procedure Dealing with Checkerboard, Mesh-Dependencies and Local Minima”, Structural Optimization, Vol. 16, pp. 68-75.

Talischi, C. et al., 2012, “PolyTop: a Matlab Implementation of a General Topology Optimization Framework Using Unstructured Polygonal Finite Element Meshes”, Struct. and Multidisc. Optim., Vol. 45, No. 3, pp. 329-357.

Versteeg, H. K. and Malalasekera, W., 1995, “An Introduction to Computational Fluid Dynamics: The Finite Volume Method”, Ed. Longman Scientific & Technical, New York, United States, 267 p.

## RESPONSIBILITY NOTICE

The authors are the only responsible for the printed material included in this paper.